

Three puzzles from nuclear astrophysics

W. C. Haxton

Department of Physics, University of California, Berkeley, and Lawrence Berkeley National Laboratory, MC-7300, Berkeley, CA 94720

E-mail: haxton@berkeley.edu

Abstract. I discuss three open problems in astrophysics where nuclear physics can make important contributions: the solar abundance problem, dark matter particle detection, and the origin of the r-process elements.

It is a great pleasure to take part in this celebration of Jerry Draayer's career in physics and to describe three problems in nuclear astrophysics that I find of interest. The descriptions here will be brief, as detailed recent references are available. The topics are 1) the solar abundance problem and its implications for the solar model and future solar neutrino experiments; 2) the elastic scattering of dark matter (DM) particles off nuclei; and 3) the possibility that an early, neutrino-driven r-process (rapid-neutron-capture process) could, in combination with neutron star mergers, account for what we know about the galactic evolution of r-process metals.

1. The solar abundance problem

The Standard Solar Model (SSM) [1, 2] assumes a homogeneous zero-age Sun because of the assumption that the proto-Sun passed through a fully convective Hayashi phase during gas-cloud collapse. The initial composition is divided into hydrogen X_{ini} , helium Y_{ini} , and metals Z_{ini} . The relative abundances of the metals (elements heavier than helium) can be taken from meteoritic data (refractory elements) and from analyses of photospheric absorption lines (volatiles such as C, N, O, Ne, Ar). As $X_{\text{ini}} + Y_{\text{ini}} + Z_{\text{ini}} = 1$, the initial solar composition can be fully specified by adjusting Y_{ini} , Z_{ini} , as well as one other parameter, the mixing length α_{MLT} , until the SSM, evolved forward by 4.6 Gyrs, reproduces the present solar radius R_{\odot} , luminosity L_{\odot} , and surface helium abundance Y_S . The metals are important contributors to the opacity and consequently influence a variety of solar properties.

Traditionally the analysis of photospheric absorption lines was done with a 1D model that did not explicitly take into account surface stratification, velocities, and inhomogeneities [3]. More recently 3D parameter-free methods have been introduced, improving the consistency of line analyses [4]. This approach led to a significant reduction in Z_{ini} , from ~ 0.0169 to ~ 0.0122 , a change that makes the Sun more consistent with similar stars in the local neighborhood. However the agreement between the SSM and various helioseismic properties, such as the sound speed profile and the location of the convective zone boundary, deteriorated with the reduced Z_{ini} (see Fig. 1). The high-energy ^8B neutrino flux is also affected, with the high-metallicity GS98-SFII SSM flux being $\sim 22\%$ higher than low-metallicity AGSS09-SFII SSM flux [2].

The solar abundance problem can be summarized as follows: There is a significant discrepancy between a SSM tuned to our best description of the solar surface (a 3D treatment of

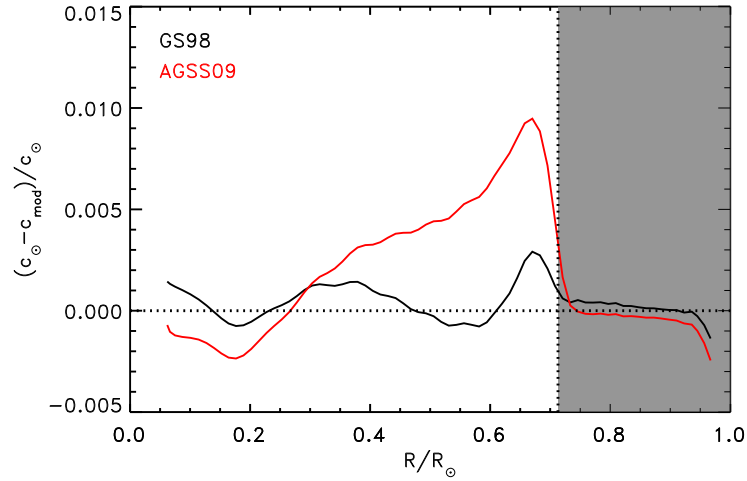


Figure 1. The differences between the sound-speed profile determined from helioseismology and those predicted by the high-metallicity GS98-SFII and low-metallicity AGSS09-SFII SSMs.

photoabsorption lines) and one tuned to reproduce properties of the solar interior (helioseismic observables). The two models have very different Z_{iniS} .

This problem is potentially related to two others illustrated in Fig. 2. The first is the anomalous composition [6] of the gaseous giant planets, Jupiter, Saturn, Uranus, and Neptune. Jupiter and Saturn are enriched in C and N by factors of 4-7, relative to the Sun. The process of planetary formation, which is thought to have occurred late in the evolution of the solar system when only $\sim 5\%$ of the nebular gas remained in a thin disk, appears to have scoured approximately 40-90 earth masses (M_{\oplus}) of metal from the disk [5]. The second comes from comparing the Sun's composition with that of solar twins [7], where systematic differences in metal abundances track condensation temperatures, with the solar ratio of volatiles to refractories being 0.05 to 0.10 dex higher than the average twin ratio.

These three problems could have a common origin, planetary disk processes that concentrate ice, dust, and other metal-rich material in the planets. If the depleted gas from which the metals were scrubbed were deposited onto the Sun after the Sun had developed its radiative core (so that the convective envelope at the time resembled the modern one, which contains less than 3% of the Sun's mass), then significant dilution of the convective zone could have occurred. This could produce a Sun with a higher metallicity radiative core and lower metallicity convective surface, invalidating the SSM's assumption of zero-age homogeneity. (Indeed, the excess metal in the planets is similar to the net difference in GS98-SFII and AGSS09-SFII SSM convective-zone metal, about $40 M_{\oplus}$.)

There has been a significant amount of recent work focused on this conjecture. The nuclear physics connections include:

- (i) Neutrino flux measurements that are sensitive to changes in solar core temperature T_c of 1%, and thus to metallicity differences comparable to those being debated.
- (ii) The development of accreting nonstandard solar models (NSSMs), and the demonstration that such models are sharply constrained by solar neutrino and helioseismic measurements.
- (iii) The possibility that future solar neutrino flux measurements could provide a direct measurement of the C+N content of the solar core.

In the case of the neutrino fluxes, the most sensitivity to T_c is exhibited by the ^8B neutrinos. However, despite current measurements that determine this flux to $\sim 3\%$ and despite SSM model

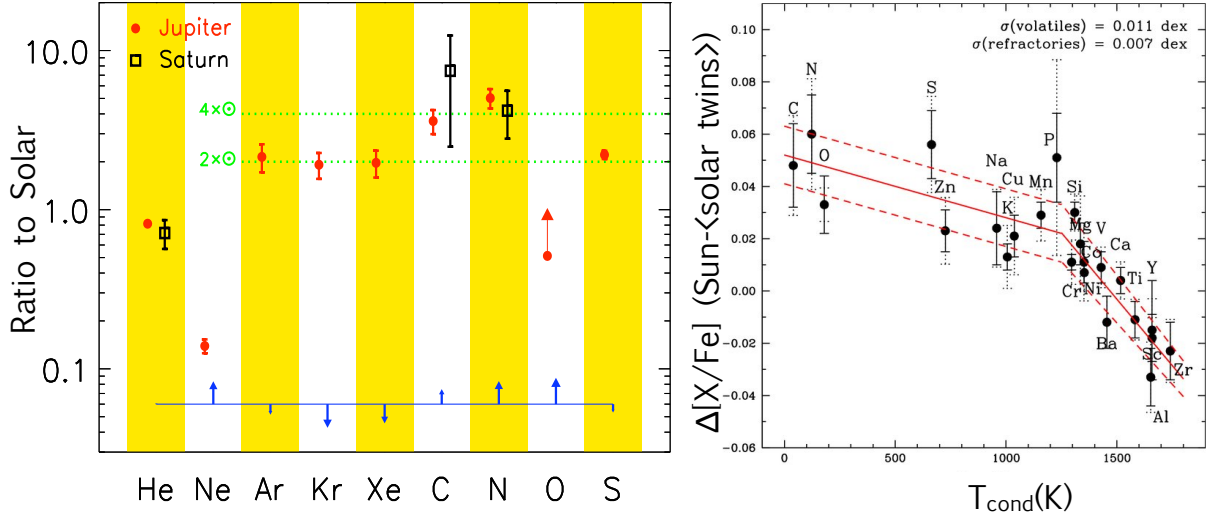


Figure 2. Left panel: Data from the Galileo and Cassini missions showing abundances in the gaseous atmospheres of Jupiter and Saturn, relative to solar. From [5]. Right panel: Deviation between solar metallicities, normalized to iron, from corresponding average quantities for solar twins, displayed as a function of the condensation temperature of the metal. From [7].

uncertainties of $\sim 14\%$ in this flux that exceed the nominal discrepancy of nearly 22% between the competing models [2], little can be concluded: the AGSS09-SFII and GS98-SFII SSM global fits to the solar neutrino data have identical χ^2 s. A metallicity intermediate between the two models would optimize the fit.

The impact of accretion on both neutrino fluxes and helioseismic variables has been evaluated in NSSMs. The work to date [8] varied the time, mass, and composition of the accreted material, but has not allowed the composition to vary in time – a simplification that one could question in view of the right panel of Fig. 2. The results are summarized in Figs. 10 and 11 of [2]. Helioseismic and neutrino observables tightly constrain such NSSMs. The envisioned candidate solution to the solar abundance problem – a low-Z surface consistent with AGSS09 abundances and a high-Z interior consistent with GS98 abundances – can be achieved with metal-free or metal-poor accretion and modest accreted masses $M_{\text{ac}} \sim 0.01 M_{\odot}$. Such models can bring the surface helium abundance into agreement with the data and produce some improvement in the sound-speed figure-of-merit $\langle \delta c/c \rangle$ and in the comparison of model and measured neutrino fluxes. However the lower surface metallicity that accompanies such models forces the convective-zone boundary R_S to move outward, contradicting results from helioseismology.

The third point above – checking interior solar abundances by using solar neutrinos as a probe – is possible because of the CN neutrinos. While the Sun produces 99% of its energy through the pp chain, proton burning also takes place through the CN I cycle, which produces significant fluxes of ^{13}N ($\sim 2.9 \times 10^8/\text{cm}^2/\text{s}$) and ^{15}O ($\sim 2.2 \times 10^8/\text{cm}^2/\text{s}$) neutrinos. These fluxes, like the ^8B neutrino flux, are very sensitive to T_c , which can be changed by varying any of the approximately 19 SSM input parameters, according to their assigned uncertainties. These uncertainties include the abundances of key metals. But in addition to the response in T_c due to changes in metallicity, the CN cycle has an additional linear dependence on the C+N abundance because these elements catalyze the proton burning.

In [9] a strategy for using the neutrino flux to measure the core C+N content was developed in which a weighted ratio of ^{15}O and ^8B fluxes is formed that is nearly independent of T_c , isolating

this linear dependence on C+N. The result (including recent improvements in the analysis) is

$$\frac{\phi(^{15}\text{O})}{\phi(^{15}\text{O})_{\text{SSM}}} = \left[\frac{\phi(^{8}\text{B})}{\phi(^{8}\text{B})_{\text{SSM}}} \right]^{0.729} x_{\text{C+N}} [1 \pm 0.006(\text{SSM}) \pm 0.027(\text{D}) \pm 0.099(\text{nucl}) \pm 0.032(\theta_{12})]. \quad (1)$$

The first factor on the right – effectively our T_c “thermometer” – is now known experimentally to 2%. The uncertainty denoted “SSM” reflects the effects on this relationship when 18 of 19 SSM input parameters are varied. The response of 0.6% reflects the success in constructing a T_c -independent relationship. But there is sensitivity to the 19th parameter, the diffusion coefficient D: Eq. (1) relates a contemporary neutrino flux measurement to the primordial C+N abundance. The composition of the modern Sun’s core is altered by the gravitational settling of C+N over 4.6 Gyr, an effect that the SSM predicts is uncertain to 2.7%. The dominant uncertainty in Eq. (1) of 9.9% comes from nuclear physics, particularly the S-factors for $^7\text{Be}(p,\gamma)$ and $^{14}\text{N}(p,\gamma)$. These S-factor uncertainties can be reduced [10]: with a factor-of-two improvement, nuclear physics would no longer dominate the error analysis. Finally there is a 3.2% uncertainty due to weak interaction parameters.

On the left appears a flux that is currently not measured, but could be determined to a precision of about 7% in the upcoming solar neutrino experiment SNO+ [11], a larger and significantly deeper version of Borexino. The depth – the experiment is under construction in the former SNO cavity at SNOLab – is important, potentially reducing backgrounds due to cosmogenic ^{11}C by a factor of ~ 70 , relative to Borexino. When all errors are combined in quadrature, one finds that the solar core abundance of C+N could be determined to $\sim 13\%$, which can be compared to the current debate over differences in Z_{ini} of $\gtrsim 30\%$.

SNO+ could allow, for the first time in stellar astrophysics, a direct experimental comparison between core and surface compositions, thereby testing the SSM assumption of initial homogeneity. If it were shown that planetary formation affects host-star surface metallicity in a characteristic way – e.g., producing an elevated ratio of volatiles to refractories – this could be important in identifying stars that are more likely to host planets.

2. The nuclear physics of dark matter detection

Several independent astrophysical observations suggest that 85% of gravitating matter is dark, residing beyond the Standard Model. This DM must be long-lived or stable, and must lack strong couplings to itself and to baryons. A leading candidate for the DM is weakly interacting massive particles (WIMPs), slow-moving massive particles (e.g., 10 GeV to 1 TeV) that can elastically scatter off nuclear targets, transferring significant momentum (~ 100 MeV). Such DM particles can be detected through nuclear recoil in carefully designed detectors mounted in low-background environments, deep underground [12].

Indeed, there is a great deal of experimental activity in DM detection, including several claims of possible discovery, and disagreements among experimentalists about the compatibility of the claims with existing limits. Various natural targets are being used, containing isotopes such as ^{19}F , ^{23}Na , $^{70,72,73,74,76}\text{Ge}$, ^{127}I , and $^{128,129,130,131,132,134,136}\text{Xe}$. Thus targets include isotopes sensitive to vector ($J \geq 1/2$) and tensor ($J \geq 1$) interactions, such as $^{19}\text{F}(1/2^+)$ and $^{129}\text{Xe}(1/2^+)$; and $^{23}\text{Na}(3/2^+)$, $^{73}\text{Ge}(9/2^+)$, $^{127}\text{I}(5/2^+)$, and $^{131}\text{Xe}(3/2^+)$.

DM particles could in principle scatter off any scalar, vector, or tensor static nuclear moment. However analyses almost always treat the nuclear response in the point-nucleus limit, despite momentum transfers comparable to the inverse nuclear size, so that the scattering is

$$\text{spin – independent (S.I.)} \Rightarrow \langle g.s. | \sum_{i=1}^A (a_0^F + a_1^F \tau_3(i)) | g.s. \rangle \quad \text{or}$$

$$\text{spin - dependent (S.D.)} \Rightarrow \langle g.s. | \sum_{i=1}^A \vec{\sigma}(i) (a_0^{GT} + a_1^{GT} \tau_3(i)) | g.s. \rangle. \quad (2)$$

Most often theoretical treatments are “top-down” – calculations motivated by a specific high-energy theory, for which a nuclear response involving a S.I. or S.D. response is then derived.

Recently a different approach was taken in which the most general Galilean-invariant effective DM-nucleon interaction was derived, including operators up to quadratic order in momenta and exchanges of particles of spin-1 or less [13]. That interaction has 11 couplings ($\times 2$ if isospin is included), in contrast to the S.I. and S.D. cases discussed above:

$$\begin{aligned} L_{ET} = & a_1 1 + a_2 \vec{v}^\perp \cdot \vec{v}^\perp + a_3 \vec{S}_N \cdot (\vec{q} \times \vec{v}^\perp) + a_4 \vec{S}_\chi \cdot \vec{S}_N + ia_5 \vec{S}_\chi \cdot (\vec{q} \times \vec{v}^\perp) + a_6 \vec{S}_\chi \cdot \vec{q} \vec{S}_N \cdot \vec{q} \\ & + a_7 \vec{S}_N \cdot \vec{v}^\perp + a_8 \vec{S}_\chi \cdot \vec{v}^\perp + ia_9 \vec{S}_\chi \cdot (\vec{S}_N \times \vec{q}) + ia_{10} \vec{S}_N \cdot \vec{q} + ia_{11} \vec{S}_\chi \cdot \vec{q} \end{aligned} \quad (3)$$

Here \vec{S}_N and \vec{S}_χ are the nucleon and DM particle spin, \vec{q} is the three-momentum transfer, and \vec{v}^\perp is the Galilean-invariant velocity operator defined in [13]. The coefficients of the eleven effective operators include an isospin dependence that has been suppressed, e.g., $a_1 \equiv a_1^0 + a_1^1 \tau_3(i)$, to allow for arbitrary couplings to protons and neutrons.

This starting point provides a vehicle for determining the corresponding most general elastic nuclear response, using the prescription that A-body nuclear currents and charges are the sums over the corresponding one-body nucleon currents and charges. One finds

$$\begin{aligned} H_{ET} = & \sum_{i=1}^A \left[l_0(i) \delta(\vec{x} - \vec{x}_i) + l_0^A(i) \frac{1}{2M} \left(-\frac{1}{i} \overleftarrow{\nabla}_i \cdot \vec{\sigma}(i) \delta(\vec{x} - \vec{x}_i) + \delta(\vec{x} - \vec{x}_i) \vec{\sigma}(i) \cdot \frac{1}{i} \overrightarrow{\nabla}_i \right) \right. \\ & + \vec{l}_5(i) \cdot \vec{\sigma}(i) \delta(\vec{x} - \vec{x}_i) + \vec{l}_M(i) \cdot \frac{1}{2M} \left(-\frac{1}{i} \overleftarrow{\nabla}_i \delta(\vec{x} - \vec{x}_i) + \delta(\vec{x} - \vec{x}_i) \frac{1}{i} \overrightarrow{\nabla}_i \right) \\ & \left. + \vec{l}_E(i) \cdot \frac{1}{2M} \left(\overleftarrow{\nabla}_i \times \vec{\sigma}(i) \delta(\vec{x} - \vec{x}_i) + \delta(\vec{x} - \vec{x}_i) \vec{\sigma}(i) \times \overrightarrow{\nabla}_i \right) \right] \end{aligned} \quad (4)$$

Here each of the associated WIMP amplitudes is a function of the various a_i appearing in Eq. (3) (including the isospin dependence), e.g.,

$$\begin{aligned} l_0(i) = & \left(a_1^0 - i(\vec{q} \times \vec{S}_\chi) \cdot \vec{v}_T^\perp a_5^0 + \vec{S}_\chi \cdot \vec{v}_T^\perp a_8^0 + i\vec{q} \cdot \vec{S}_\chi a_{11}^0 \right) \\ & + \left(a_1^1 - i(\vec{q} \times \vec{S}_\chi) \cdot \vec{v}_T^\perp a_5^1 + \vec{S}_\chi \cdot \vec{v}_T^\perp a_8^1 + i\vec{q} \cdot \vec{S}_\chi a_{11}^1 \right) \tau_3(i) \equiv l_0^0 + l_0^1 \tau_3(i). \end{aligned} \quad (5)$$

Equation (4) involves five nuclear densities, each of which is familiar from studies of semi-leptonic electroweak interactions,

- (i) The isoscalar and isovector vector charge operators $\rho_V^0(\vec{x}) = \sum_{i=1}^A \delta(\vec{x} - \vec{x}_i)$ and $\rho_V^1(\vec{x}) = \sum_{i=1}^A \delta(\vec{x} - \vec{x}_i) \tau_3(i)$ familiar from elastic electron scattering;
- (ii) The isoscalar axial-vector charge operator $\rho_A^0(\vec{x}) = \sum_{i=1}^A \frac{1}{2M} \left(-\frac{1}{i} \overleftarrow{\nabla}_i \cdot \vec{\sigma}(i) \delta(\vec{x} - \vec{x}_i) + \delta(\vec{x} - \vec{x}_i) \vec{\sigma}(i) \cdot \frac{1}{i} \overrightarrow{\nabla}_i \right)$ and the corresponding isovector operator that mediates axial-charge $0^+ \leftrightarrow 0^-$ β decay;
- (iii) The isoscalar axial-vector spin operator $\vec{j}_A^0(\vec{x}) = \sum_{i=1}^A \vec{\sigma}(i) \delta(\vec{x} - \vec{x}_i)$ and its isovector counterpart, familiar from inelastic neutrino reactions in the long-wavelength limit (LWL);
- (iv) The isoscalar vector velocity current $\vec{j}_{V,v}^0(\vec{x}) = \sum_{i=1}^A \frac{1}{2M} \left(-\frac{1}{i} \overleftarrow{\nabla}_i \delta(\vec{x} - \vec{x}_i) + \delta(\vec{x} - \vec{x}_i) \frac{1}{i} \overrightarrow{\nabla}_i \right)$ and its isovector counterpart, familiar from electron scattering; and

	even	odd
vector	C_0	C_1
axial	C_0^5	C_1^5

	even	odd	even	odd	even	odd
axial spin	L_0	L_1^5	T_2^{el}	$T_1^{5\text{el}}$	T_2^{mag}	$T_1^{5\text{mag}}$
vector velocity	L_0	L_1	T_2^{el}	T_1^{el}	T_2^{mag}	T_1^{mag}
vector spin – velocity	L_0	L_1	T_2^{el}	T_1^{el}	T_2^{mag}	T_1^{mag}

Response Type	Long-wavelength Limit
$C_{J=\text{even},M}$	$\frac{1}{\sqrt{4\pi}}1(i)$
$L_{J=\text{odd},M}^5$	$\frac{1}{2\sqrt{3\pi}}\sigma_{1M}(i)$
$T_{J=\text{odd},M}^{\text{el}5}$	$\frac{1}{\sqrt{6\pi}}\sigma_{1M}(i)$
$T_{J=\text{odd},M}^{\text{mag}}$	$-\frac{q}{2m_N\sqrt{6\pi}}\ell_{1M}(i)$
$L_{J=\text{even},M}$	$-\frac{q}{3m_N\sqrt{4\pi}}\vec{\sigma}(i) \cdot \vec{\ell}(i);$ $-\frac{q}{m_N\sqrt{30\pi}}[x_i \otimes (\vec{\sigma}(i) \times \frac{1}{i}\vec{\nabla})_1]_{2M}$
$T_{J=\text{even},M}^{\text{el}}$	$-\frac{q}{m_N\sqrt{20\pi}}[x_i \otimes (\vec{\sigma}(i) \times \frac{1}{i}\vec{\nabla})_1]_{2M}$

Figure 3. Left: Parity and time-reversal constraints on multipoles mediating WIMP elastic scattering. Only the lowest even and lowest odd multipoles are shown, as all even and all odd multipoles transform similarly. Multipoles eliminated by parity (time reversal) are indicated by a red (blue) strike. Right: Table of the surviving parity- and time-reversal-allowed responses, and their LWLs.

- (v) The isoscalar vector spin-velocity current $\vec{J}_{V,sv}^0(\vec{x}) = \sum_{i=1}^A \frac{1}{2M} \left(\vec{\nabla}_i \times \vec{\sigma}(i) \delta(\vec{x} - \vec{x}_i) + \delta(\vec{x} - \vec{x}_i) \vec{\sigma}(i) \times \vec{\nabla}_i \right)$ and its isovector counterpart.

The vector spin-velocity current appears in Serot’s [14] treatment of semi-leptonic electroweak interactions to order $1/M^2$. In that context, because of the properties of this current under time reversal, it is accompanying by a factor of the energy transfer q_0 that vanishes for elastic transitions.

Equation (4) follows from L_{ET} , but could have been written down directly as a nuclear-level effective theory, as it includes all possible local one-body operators of rank ≤ 1 that can be constructed with $\vec{\sigma}$, τ_3 , and one gradient.

Nuclear ground states are approximate eigenstates of parity and time-reversal. Thus, ignoring small components of the wave function that break these symmetries, one should retain only multipoles generated from the nuclear densities that transform appropriately under parity and time reversal. The charge operators of Eq. (4) generate even and odd multipoles: because all even and all odd multipoles transform similarly, it is sufficient to consider only the $J=0$ and $J=1$ cases. The current operators generate longitudinal, transverse electric, and transverse magnetic multipoles. Again, we can limit our consideration to the lowest contributing even and odd multipoles, as the generalization to other cases is immediate. The multipoles eliminated by symmetry considerations are indicated in Fig. 3.

Fig. 3 also gives the LWLs of the surviving multipoles, which are even vector charge operators (C_0, C_2, \dots), even vector spin-velocity longitudinal operators (L_0, L_2, \dots), odd axial spin longitudinal operators (L_1^5, L_3^5, \dots), even vector spin-velocity electric operators ($T_2^{\text{el}}, T_4^{\text{el}}, \dots$), odd axial spin electric operators ($T_1^{5\text{el}}, T_3^{5\text{el}}, \dots$), and odd vector spin magnetic operators ($T_1^{\text{mag}}, T_3^{\text{mag}}, \dots$). Thus there are six independent response functions – not simply the two (S.D., S.I.) conventionally treated.

The $C_{J=\text{even},M}$ operator of Fig. 3 is the standard S.I. response, while $L_{J=\text{odd},M}^5$ and $T_{J=\text{odd},M}^{\text{el}5}$ are the longitudinal and transverse components that are usually summed to give the S.D. response. These two contributors to the S.D. response have distinct form factors and couple in distinct ways to WIMP amplitudes, however. The transverse magnetic response $T_{J=\text{odd},M}^{\text{mag}}$ is new, generated by the vector velocity current. In the LWL the operator is proportional to the nuclear orbital angular momentum operator $\vec{\ell}(i)$, and thus is explicitly connected with the

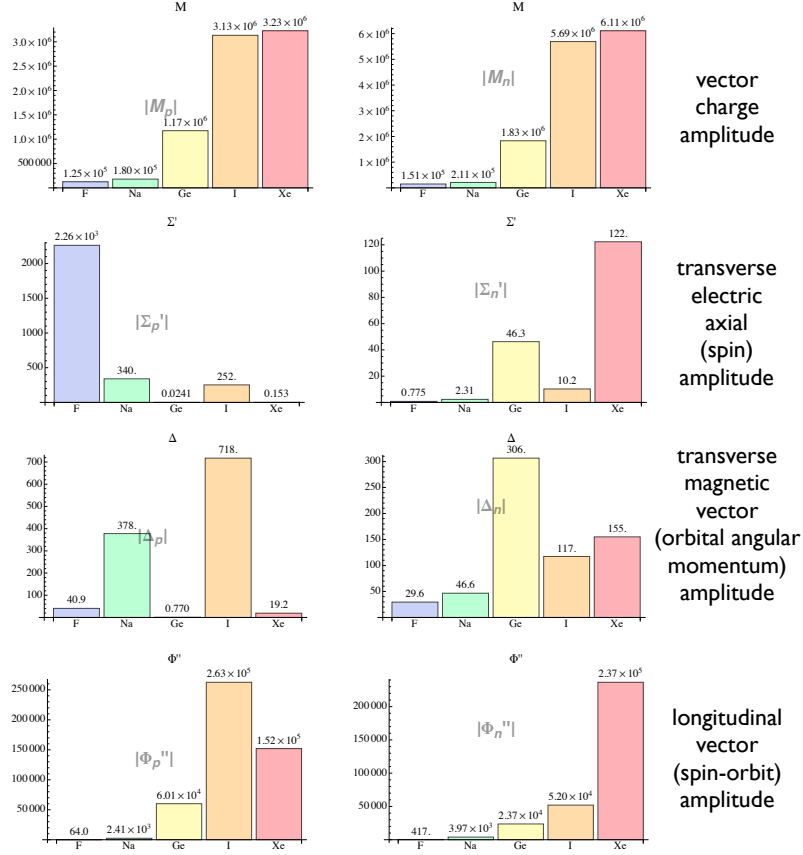


Figure 4. Magnitudes of response function amplitudes are compared for four of the response functions discussed in the text (the S.I. vector response, the S.D. transverse electric axial response, the transverse magnetic vector response, and the longitudinal vector response). The isospin couplings are to protons only (left panels) and neutrons only (right panels). From [13].

composite nature of the nucleon (apparent from the accompanying factor of q in the right panel of Fig 3). Thus there are three responses – one proportional to $\vec{\ell}$ and two proportional to $\vec{\sigma}$ in the LWL – that transform under rotations as $\langle J_i | \vec{J}_M | J_i \rangle$. The fifth and sixth responses of Fig. 3 are generated by the spin-velocity current and also reflect nucleon compositeness. They transform as longitudinal and transverse electric projections of the vector spin-velocity current $\sim \delta(\vec{x} - \vec{x}_i) \vec{\sigma}(i) \times \vec{\nabla}$, respectively – just as the two S.D. responses arise as the longitudinal and transverse electric projections of the axial spin current. The first, $L_{J=\text{even}, M}$, generates a scalar nuclear response proportional to the spin-orbit interaction $\vec{\sigma}(i) \cdot \vec{\ell}(i)$ as well as a tensor contribution, in the LWL. The scalar response is present for all nuclei (that is, regardless of ground-state spin, like the S.I. charge coupling). But its properties are very different from those of the S.I. operator: $\vec{\sigma}(i) \cdot \vec{\ell}(i)$ produces a coherent isoscalar contribution over closed spin-orbit partner shells, e.g., the closed $1f_{7/2}$ shell for Ge isotopes and the closed $1g_{9/2}$ shell for Xe or I. The sixth response function, $T_{J=\text{even}, M}^{\text{el}}$, is the transverse electric projection of the spin-velocity current.

Figure 4 shows response functions calculated in the shell model for natural targets of F, Na, Ge, I, and Xe [13] – these responses could be labeled as S.I., S.D. (transverse axial electric), orbital angular momentum, and spin-orbit, in the LWL. Very large differences in experimental

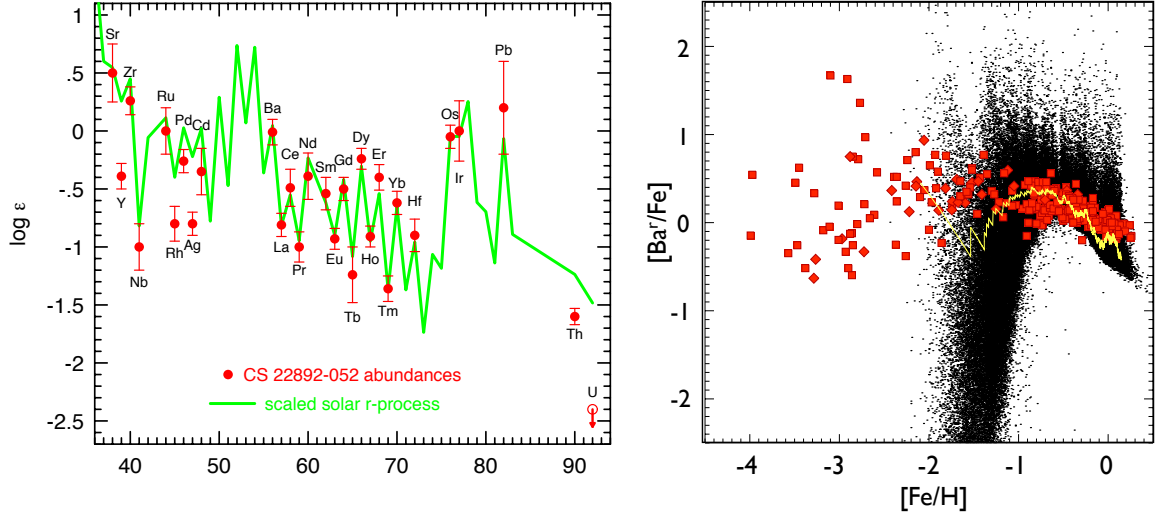


Figure 5. Left: Metal abundances from metal-poor halo star CS 22892-052 compared to the scaled solar distribution. From [17]. Right: The observed r-process fraction of Ba relative to Fe (red squares and diamonds) as a function of $[\text{Fe}/\text{H}]$, compared to the model calculations (black dots) of the evolution in the galactic rate of neutron star mergers, assuming an average merger rate of 20/Myr and a coalescence timescale of 1 Myr. From [18].

sensitivity appear between detector materials, as the interaction and thus the response is varied – the space of possibilities is much larger than in the standard S.I./S.D. description. One might think this is unfortunate – the correlations between different experiments will be harder to anticipate – but I would argue with this view. We know nothing about DM interactions, but we know a lot about nuclear responses. The six nuclear responses provide six nuclear dials that can be used to probe the nature of DM. The experimental DM community might benefit from greater interaction with the nuclear physics community, in formulating strategies for exploiting the available nuclear responses to determine DM particle properties.

3. The search for the r-process site

The search for the site or sites of the r-process, the rapid-neutron-capture process thought to be responsible for synthesizing about half the heavy elements, has been a long and frustrating one. For the past two decades the leading candidate site [15] has been the neutrino-driven wind that blows off the proto-neutron star surface in a core-collapse supernova. As the slightly neutron-rich, high-entropy nucleon gas expands off the star and cools, the protons are locked up in an alpha freeze-out. A small number of seed nuclei can be synthesized through alpha-induced reactions. The remaining free neutrons then capture on these seeds to produce heavy nuclei. If the necessary neutron/seed ratio of $\gtrsim 100$ can be maintained, the synthesis can continue up to the transuranics.

Unfortunately a number of difficulties have arisen in explorations of the neutrino-wind mechanism. It is difficult to keep the number of seeds from growing due to reactions such as $\alpha + \alpha + n \rightarrow {}^9\text{Be} + \gamma$ and $3\alpha \rightarrow {}^{12}\text{C} + \gamma$. It is also difficult to maintain the needed neutron fluence. The wind is needed as the ejection mechanism, but every $\nu_e + n \rightarrow p + e^-$ reaction results in the net loss of two neutrons via $2n + 2p \rightarrow {}^4\text{He} + \gamma$. Consequently, it was recently concluded that the net production in the standard neutrino wind scenario was limited to some $N=50$ closed-shell nuclei and to some light p-nuclei [16].

This presents quite a puzzle. While there is an alternative and very attractive site that could be responsible for the bulk of the r-process material found in the Milky Way – neutron star mergers – it is unlikely that this mechanism can account for the r-process patterns we see in certain old, metal-poor halo stars (left panel, Fig. 5). Few neutron-star mergers are expected at low metallicity because it takes time for the progenitor stars to evolve, as the right panel of Fig. 5 shows. Furthermore, because metal-poor stars sample the r-process locally at a time when the galaxy is chemically inhomogeneous, one can estimate the rate of r-process events in the early galaxy from the fluctuations in observed abundances. One finds $\sim 10^{-2}/\text{y}$. While the uncertainty in this estimate is large, the rate is typical of core-collapse supernovae and much higher than would be expected for neutron star mergers, even today.

Studies of metal-poor stars have been the main source of new information on the r-process. The metals on the surfaces of such stars are thought to have arisen from a single, or perhaps a few, nearby r-process sites. The correspondence between the abundances in such stars and the scaled r-process distribution of our Sun (left panel, Fig. 5) suggests that the r-process distribution produced in a single event is similar to that averaged over many events.

Because of the difficulty of finding a robust r-process that naturally accounts for both the metal-poor-star data and integrated r-process yields, my collaborators and I recently explored another scenario:

- One r-process component that operates at early times, is associated with supernovae, and depends on the low-metallicity environments found in early massive stars. This early r-process would need to account for the metal-poor-star r-process abundance pattern and the observed local enrichments. It would need to operate until a metallicity of -2.5 to -2.0, the time a more robust r-process would then take over.
- The second process, unconstrained by the metal-poor star data but possibly responsible for the bulk of r-process synthesis, would then need to turn on in a manner consistent with r-process chemical evolution studies. Neutron-star mergers would be the natural candidate for this second r-process.

There is also a candidate mechanism for the first r-process, neutrons produced by neutrino reactions in the He shell of a type II supernova [19]. This mechanism was originally suggested as “the r-process,” studied in high-metallicity stars, and found to fail there because the neutron/seed ratio was about a factor of 20 too low [20]. This failure reflected both the relatively weak neutron source and the high abundance of neutron poisons such as ^{14}N in the He shells of the progenitor stars that were studied. The mechanism exploits the fact that neutrons scatter off He without capturing, and thus have an enhanced probability of capture on Fe and other heavy seeds.

We re-examined this r-process in the context of metal-poor stars, using a library of progenitors generated with the Kepler code, and constructing more complete reaction networks. The details are given in [21]. Many of the conclusions of earlier studies were altered: the nuclear physics operated differently (for example, neutral-current production of neutrons was found to be unimportant), and the effects of neutron poisons were found to be less severe. Most important, the study included the effects of neutrino oscillations. With the assumption of an inverted hierarchy and a relatively hard heavy-flavor neutrino spectrum, neutron abundances of $\sim 10^{19}/\text{cm}^3$ were produced and maintained for long times in a variety of stars.

The mechanism is unusual: It is a cold r-process, with equilibrium established by neutron capture $\leftrightarrow \beta$ decay, and with a path farther from the neutron-drip line than in hot r-processes like the ν -driven wind. This has consequences for the abundance pattern and for the time-development of the r-process (see Fig. 6). The time scales are exceptionally long, with the third peak forming only after ~ 20 seconds. Furthermore, synthesis continues after passage of the shock wave, augmented by the compression of the He shell and extending to times ~ 60 seconds

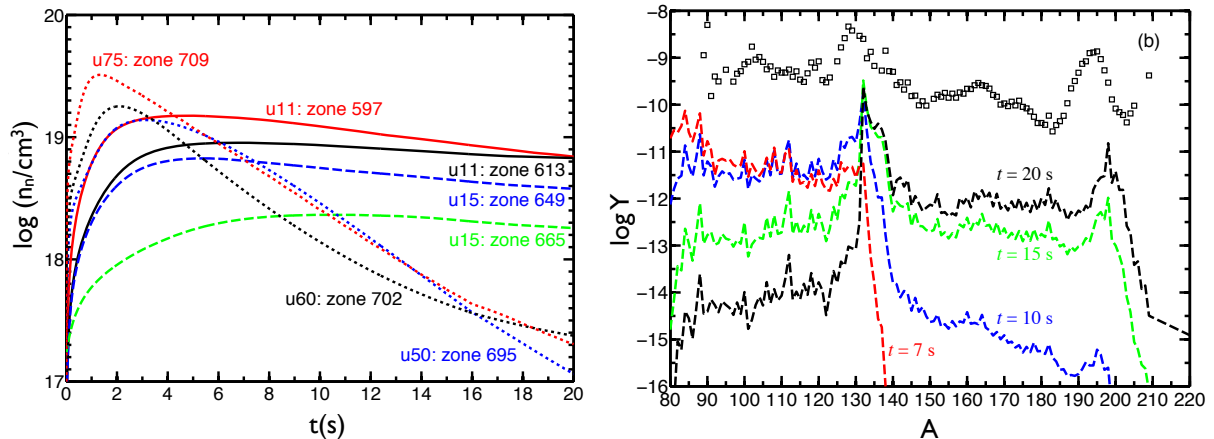


Figure 6. Left: Neutron number densities as a function of time generated by neutrino interactions in the He zone of allow-metallicity iron-core supernova. The results are for specific zones in metal-poor progenitors between 11 and 75 M_\odot . Right: The resulting number fractions $Y_i(t)$ at times of 7, 10, 15, and 20 s, compared to the solar r-process pattern (squares).

(not shown in the figure). The mechanism works well for metallicities of $10^{-4} < Z < 10^{-3}$ in Fe-core supernovae between 11-16 M_\odot and for very massive progenitors of 49-75 M_\odot . It naturally accounts for some of the features seen in metal-poor stars, such as a highly variable yield in Eu/Fe. It is also interesting from the neutrino physics viewpoint, turning on (inverted) or off (normal) with the choice of hierarchy. I am not aware of any other example in astrophysics as dramatically dependent on the neutrino hierarchy.

Acknowledgement

I want to thank my key collaborators on the work reported here, including Aldo Serenelli, Liam Fitzpatrick, Ami Katz, Projjwal Banerjee, Alex Heger, and Yong Qian, as well as the organizers for the opportunity to take part in this celebration of the scientific career of a long-time friend, Jerry Draayer. This work was supported in part by the U.S. Department of Energy under contracts DE-SC00046548 (UC Berkeley) and DE-AC02-98CH10886 (LBNL).

References

- [1] Bahcall J N 1989 *Neutrino Astrophysics* (Cambridge: Cambridge University Press)
- [2] Haxton W C, Robertson R G H, and Serenelli A M 2013 *Ann. Rev. Astron. Astrophys.* **51** (in press)
- [3] Grevesse N and Sauval A J 1998 *Space Sci. Rev.* **85** 161
- [4] Asplund M, Grevesse N, Sauval A J, and Scott P 2009 *Ann. Rev. Astron. Astrophys.* **47** 481
- [5] Guillot T 2005 *Ann. Rev. Earth Planetary Sci.* **33** 493
- [6] Nordlund A 2009 Solar Twins and Possible Solutions of the Solar and Jupiter Abundance Problems arXiv:0908.3479
- [7] Melendez J, Asplund M, Gustafsson B, and Yong D 2009 *Ap. J.* **704** L66
- [8] Serenelli A M, Haxton W C, and Peña-Garay C 2011 *Ap. J.* **743** 24
- [9] Haxton W C and Serenelli A M 2008 *Ap. J.* **687** 678
- [10] Adelberger E G *et al.* 2011 *Rev. Mod. Phys.* **70** 1275
- [11] Chen M 2006 *SNO and SNO+* (AIP Conf. Proc. **944**, AIP) p 25
- [12] Feng J L 2010 *Ann. Rev. Astron. Astrophys.* **48** 495
- [13] Fitzpatrick A L, Haxton W C, Katz E, Lubbers N, and Xu Y, The Effective Field Theory of Dark Matter Direct Detection arXiv:1203.3542
- [14] Serot B 1979 *Nucl. Phys.* **A322** 408
- [15] Woosley S E and Hoffmann R D 1992 *Ap. J.* **295** 202

- [16] Roberts L F, Woosley S E, and Hoffmann R D 1992 *Ap. J.* **722** 1
- [17] Sneden C *et al.* 2003 *Ap. J.* **591** 936
- [18] Argast D, Samland M, Thielemann F-K, and Qian, Y-Z 2003 *A. & A.* **416** 997
- [19] Epstein R, Colgate S, and Haxton W C 1988 *Phys. Rev. Lett.* **61** 2038
- [20] Woosley S E, Hartmann D, Hoffman R D, and Haxton W C 1990 *Ap. J.* **356** 272
- [21] Banerjee P, Haxton W C, and Qian Y-Z 2011 *Phys. Rev. Lett* **106** 201104